Int J Clin Exp Med 2015;8(11):20046-20055
www.ijcem.com /ISSN:1940-5901/IJCEM0014291

Original Article

T1 finite element model of Kümmell's disease shows changes in the vertebral stress distribution

Yunshan Su*, Dong Ren*, Meng Jiang, Pengcheng Wang

*Orthopaedic Trauma Service Center, Third Hospital of Hebei Medical University, Major Laboratory of Orthopaedic Biomechanics in Hebei Province, Shijiazhuang, China. *Equal contributors.*

Received August 10, 2015; Accepted November 12, 2015; Epub November 15, 2015; Published November 30, 2015

Abstract: The aims of this study were to develop a finite element model of delayed post-traumatic vertebral osteonecrosis, analyze its effect on the vertebral stress distribution, and provide experimental evidence for osteonecrosis as a risk factor for loss of the vertebral corrective angle. Three-dimensional reconstruction was performed on CT data of the lumbar vertebrae from a 29-year-old male without spinal lesions to develop a normal L1-L3 vertebral model and a model with post-traumatic vertebral osteonecrosis at level L2. Vertebral flexion, extension, and lateral bending were simulated using computer software to determine the stress distribution in the cortical and cancellous bone in the two models and the changes in the vertebral stress distribution with the size and location of the cavity. Simulation of a vertebral cavity tended to increase the Von Mises equivalent stress in the vertebral cancellous bone and reduce the equivalent stress in the cortical bone, while the vertebral equivalent stress displayed a reverse distribution. The equivalent stress was increased in both the cancellous and cortical bones with increasing cavity volume, and the equivalent stress in the cortical bone was always smaller than that in the normal vertebrae. Placing the cavity close to the endplate of the vertebrae tended to cause stress concentrations in the cancellous bone around the endplate. The cancellous bone with post-traumatic osteonecrosis tended to experience greater Von Mises equivalent stress than the normal vertebrae. Differences in the cavity volume and location may result in a more severe abnormal stress distribution.

Keywords: Thoracolumbar fractures, Kümmell's disease, post-traumatic vertebral osteonecrosis, stress distribution, finite element

Introduction

Delayed post-traumatic osteonecrosis, also known as Kümmell's disease, intervertebral vacuum, and delayed vertebral collapse, was first discovered and described by Kümmell [1] in 1895. Kümmell described the disease as cavity-like changes in a vertebra that occur after vertebral fractures. Matzaroglou et al. reported that such vertebral fractures are the result of trauma followed by ischemic necrosis of the vertebral body [2]. Although a few studies have demonstrated that the vertebral height can be restored using distraction reduction in patients who have severe collapse of the thoracolumbar fractures, the mounting structure of the bone trabeculae in each vertebra cannot be regenerated at the same time, resulting in cavity-like formations in the vertebrae (**Figure 1A**) [3]. The failure to reconstruct or restore a vertebra in a timely manner after injury likely leads to fatigue fractures of the posterior internal fixation, leaving the patient prone to vertebral collapse and loss of the corrective angle after extraction of the internal fixation [4]. The incidence of traumatic osteonecrosis in such cases is approximately 11.5% [5].

Finite element analysis (FEA) is a method for simulating real physical systems using mathematical approximations and is an important approach for studying biomechanical structures. FEA has been used in many studies to optimize orthopedic and spine-related surgical implants and procedures.

The purpose of the present study was to use three-dimensional FEA to provide experimental evidence showing that post-traumatic osteonecrosis can alter the vertebral stress distribution and may be a risk factor for the loss of the vertebral corrective angle after extraction of internal fixation.

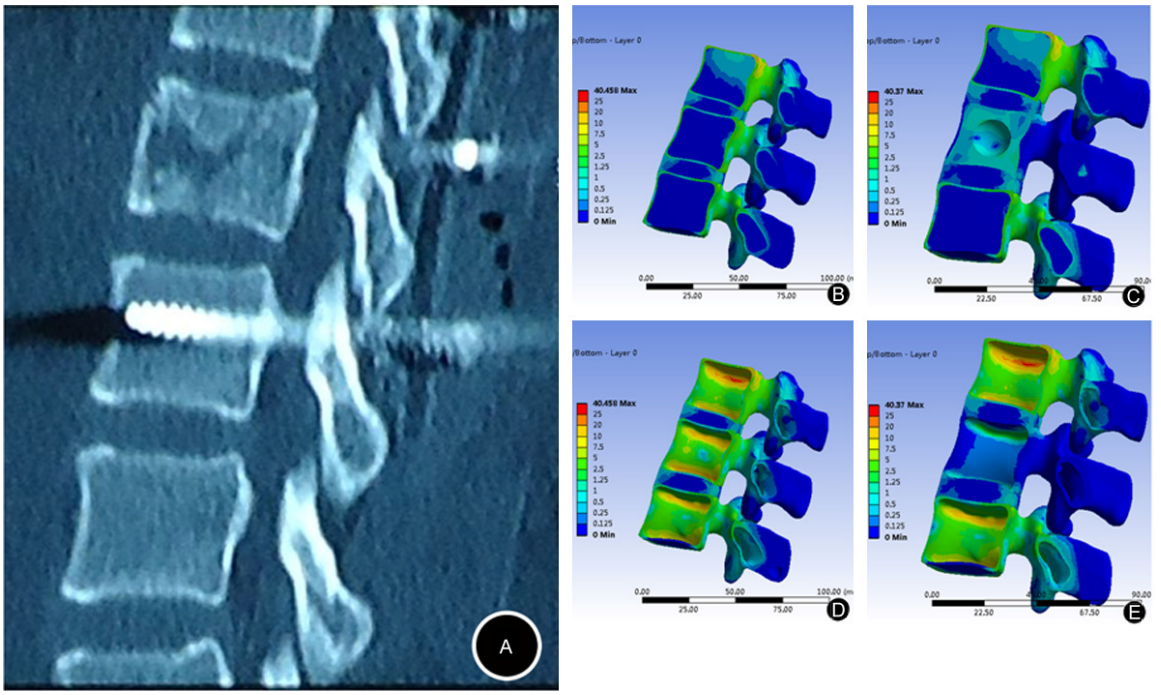

Figure 1. A. The vertebral cavity-like changes after distraction reduction treatment for thoracolumbar fractures. The irregular low density regions in the front-center area of a and middle area of b show the cavity-like changes in the vertebra. B-E. Von Mises stress distributions in the normal vertebra and cavity-like vertebra under 260 N of axial pressure and 10 Nm of left bending torque. B. Cancellous bone in a normal vertebra; C. Cancellous bone in a cavity-like vertebra; D. Cortical bone in a normal vertebra; E. Cortical bone in a cavity-like vertebra.

Table 1. Material properties of the various lumbar tissues

Structure	Elastic modulus (MPa)	Poisson ratio	Yield stress (MPa)	Sectional area (mm^2)
Vertebra				
Cortical bone	12000	0.3	2.0	-
Cancellous bone	100	0.2	100	-
Intervertebral disc				
Nucleus pulposus	0.2	0.4999	-	-
Annular fiber	450	0.3	-	0.2
Ligament				
Anterior longitudinal ligament	20.0	0.3	-	22.4
Posterior longitudinal ligament	20.0	0.3	-	7.0
Yellow ligament	19.5	0.3	-	14.1
Supraspinal ligament				10.5
Interspinal ligament				14.1
Capsule ligament				10.5
Intertransverse ligament				0.6

Materials and methods

Data collection

The study protocol was approved by the Ethics Committees of the Third Hospital of Hebei Medical University, and the participant provided written informed consent. We selected a 29-year-old healthy male volunteer, who was 175 cm tall and weighed 70 kg. He had no history of trauma or fractures and was confirmed to have no spinal lesions upon X-ray examination. A 64-slice spinal CT (Siemens, Munich, Germany) was used to scan his L1-L3 vertebral levels using a tube voltage of 120 kV, tube current of 200 mA, slice thickness of 1 mm, and interlayer spacing of 1 mm. The scanned data were exported in the DICOM format, and 197 DICOM images were obtained.

Model development

The DICOM images were imported into the interactive medical imaging control system Mimics 14.0 (Materialise, Leuven, Belgium), three-dimensional reconstruction was performed to create vertebral models of levels L1-L3, excluding the intervertebral discs and ligaments. Pedicle screws (6.5 mm in diameter

Table 2. Range of motion measured at each lumbar level under 10 Nm of torque

	Flexion		Extension		Left bending		Right bending	
	Current study	Yamamoto	Current study	Yamamoto	Current study	Yamamoto	Current study	Yamamoto
L1-L2 (°)	4.9	5.8	3.6	4.3	4.2	4.7	4.3	5.2
L2-L3 (°)	5.6	6.5	3.8	4.3	6.6	7.0	6.5	7.0

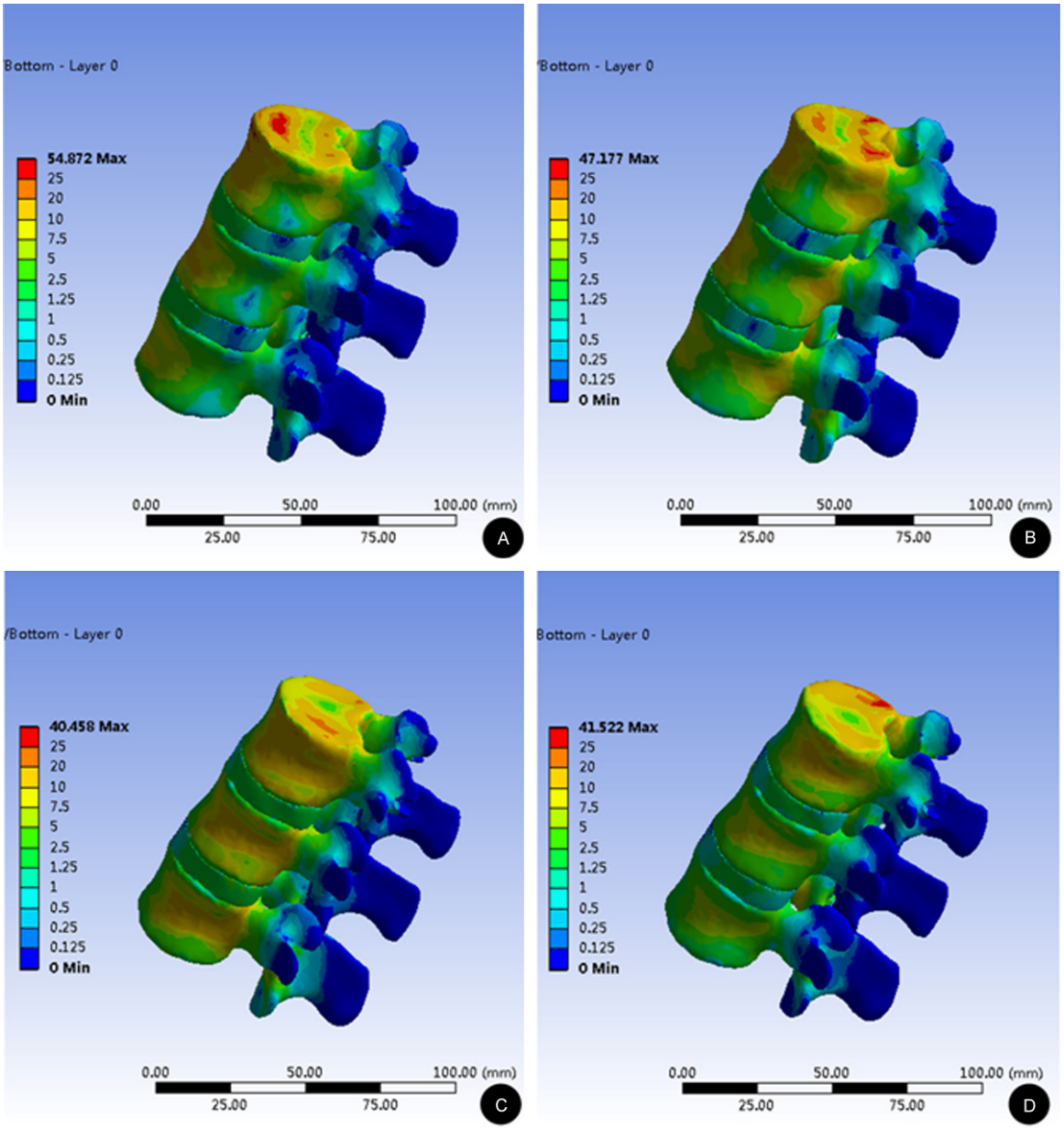

Figure 2. Von Mises stress distributions in normal vertebra under 260 N of axial pressure and 10 Nm of torque, where blue indicates low and red high Von Mises stress. The stress is concentrated in the posterior vertebra near the pedicle and is transmitted to the posterior lateral side during all four movements, where the orange and red colors indicate stress concentration areas on the flexion and bending sides. A. Flexion, B. Extension, C. Left bending, D. Right bending.

and 50 mm long) were drawn using the sketch function of the parametric modeling software Creo Parametric 2.0 (Parametric Technology Corporation, Needham, MA, USA). The screws

Table 3. Von Mises equivalent stress in the vertebral cancellous bone during flexion for different cavity sizes (MPa)

Group	Number of nodes	Quartiles of equivalent stress	*P* value
Normal vertebra	45065	0.0857 (0.0360, 0.1964)	
1/5 cavity	51914	0.7130 (0.4385, 1.3130)	P<0.001
2/5 cavity	52408	0.9017 (0.5265, 1.5400)	P<0.001
3/5 cavity	53021	0.9918 (0.5518, 1.6048)	P<0.001
4/5 cavity	53656	1.3084 (0.7765, 1.9332)	P<0.001
5/5 cavity	54290	1.9259 (0.8853, 3.4870)	P<0.001

All cavity sizes were compared with the normal vertebra.

were integrated into the L1 and L3 vertebral models in the 3-matic module of Mimics 14.0 software in the same way that lumbar pedicle screws are implanted clinically to create vertebral models with pedicle screws at the L1 and L3 levels. Next, the vertebral model and pedicle screw model were meshed separately and Boolean subtraction was performed to create vertebral models of the L1 and L3 levels in which the pedicle screws were removed. As a final step, the intervertebral discs and nuclei pulposi were added between the L1-L2 and L2-L3 vertebrae following the anatomic structure of normal human vertebrae using the automatic reverse engineering software Geomagic Studio 12.0 (3D Systems, Rock Hill, SC, USA). Other ligaments were also added, such as the anterior longitudinal, posterior longitudinal, supraspinal, interspinal, yellow, capsule, and intertransverse. In the same manner, we constructed a three-dimensional model of L1-L3 for FEA with a cavity-like vertebra at level L2. Although most of the cavities observed in cavity-like vertebrae are irregularly shaped, a sphere-shaped cavity was used here.

Meshing, contact method, and the material properties in ANSYS

The vertebra, intervertebral disc, and nucleus pulposus at each level were imported using an ANSYS pretreatment in the cdb format into the FE modeling software ANSYS Workbench. All of the developed ligaments were imported in STL format. After successful importation, the vertebra, intervertebral disc, and nucleus pulposus were meshed in ANSYS Workbench using hexahedral meshing, and the ligaments were meshed using pentahedral and hexahedral meshing, resulting in 431557 nodes and 248752 elements in the normal L1-L3 model. Contact between the facet joints was set as "no separation contact", which is defined as slight movement with no separation, and "bonded contact" was applied to the contacts between the vertebra and intervertebral disc, intervertebral disc and nucleus pulposus, and vertebra and ligaments, as well as between the intervertebral disc and the ligaments. The elastic moduli and Poisson ratios assigned to various parts of the model are listed in **Table 1** [6-8].

Model validation

Pressures of 260 N in the axial direction and 10 Nm of torque were applied to the surface of the L1 vertebra [7] to simulate the flexion, extension, and bending of the vertebra under loading. The range of motion between the two vertebrae was measured for each motion type, and the results were compared with previous results obtained from biomechanical experiments (**Table 2**). The predicted results in the present study were similar to those previously reported [9-10]. Next, the Von Mises stress distributions for the three motion types were determined (**Figure 2**). The vertebral stresses were primarily concentrated in the posterior vertebrae, presenting posterolateral conduction. These findings were also consistent with previously reported results [11-14], confirming the validity of the present model.

Loading

The bases of the L3 vertebrae and the posterior structure were fixed against all displacements and rotations. The following observations were made. (1) The stress distributions in the normal and cavity-like L2 vertebrae. (2) The vertebral stress distributions for a cavity located in the vertebral center and had a diameter of 1/5, 2/5, 3/5, 4/5, and 5/5 of the vertebral height, without breaking through the superior or inferior cortical endplates of the vertebrae. (3) The vertebral stress distributions for a cavity whose diameter was 3/5 of the vertebral height and the sphere center located within 1/3 of the vertebral width before or after the vertebral sagittal diameter, within 1/3 of the vertebral height above or below the vertical diameter, and at the center of the vertebra.

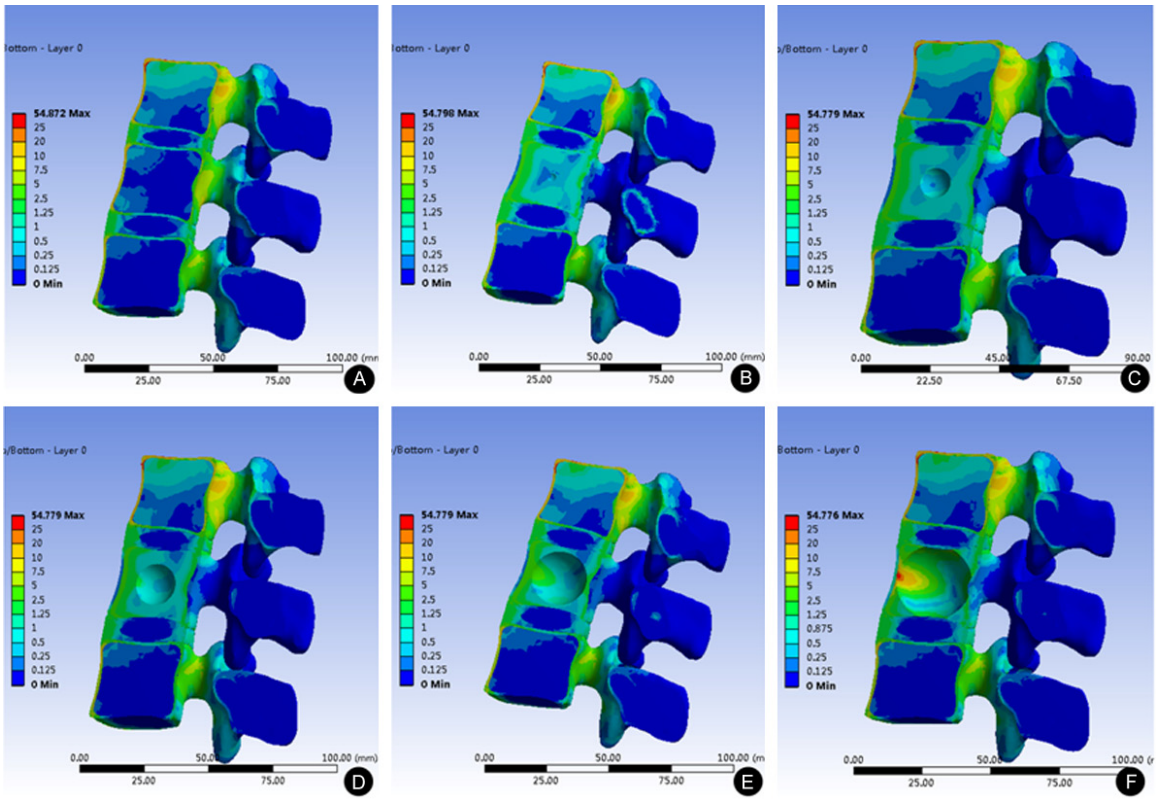

Figure 3. Von Mises stress distributions in the cancellous bone of models with different cavity sizes under 260 N of axial pressure and 10 Nm of bending torque. A. No cavity, B. 1/5 cavity, C. 2/5 cavity, D. 3/5 cavity, E. 4/5 cavity, and F. 5/5 cavity.

Table 4. Von Mises equivalent stress in the vertebral cortical bone during flexion for different cavity sizes (MPa)

Group	Number of nodes	Quartiles of equivalent stress	*P* value
Normal vertebra	32425	4.3580 (2.3650, 5.9906)	
1/5 cavity	32425	0.1566 (0.0818, 0.3085)	P<0.001
2/5 cavity	32425	0.1632 (0.0980, 0.5852)	P<0.001
3/5 cavity	32425	0.1804 (0.1033, 0.7618)	P<0.001
4/5 cavity	32425	0.2113 (0.1309, 0.9094)	P<0.001
5/5 cavity	32425	0.3690 (0.1864, 1.2157)	P<0.001

All cavity sizes were compared with the normal vertebra.

Statistical analysis

Statistical analyses were performed in SPSS 16.0 software (SPSS Company, Chicago, IL, USA). (1) The Von Mises equivalent stress at each node of the cortical and cancellous bones ahead of the bilateral pedicles in each group was compared using a multiple independent samples Kruskal-Wallis H test. If the difference was statistically significant, paired-comparisons between groups were performed using Mann-Whitney U test and an inspection level P of 0.003 was adapted after correction. (2) For the cavity diameter equal to 3/5 of the vertebral height, the Von Mises equivalent stresses at all nodes of the leading and trailing hemispheres of the cavity in models where the center of the cavity was moved along the vertebral sagittal diameter were compared using a multiple independent samples Kruskal-Wallis H test. For statistically significant effects, paired-comparisons between groups were performed using Mann-Whitney U tests with *P*-values less than 0.003 considered statistically significant. Similar statistical tests were applied to the Von Mises equivalent stresses at all nodes of the superior and inferior hemispheres of the cavity in the models where the cavity location was moved along the vertebral vertical diameter.

Results

The Von Mises equivalent stress in the cancellous bone in the cavity-like vertebra was higher

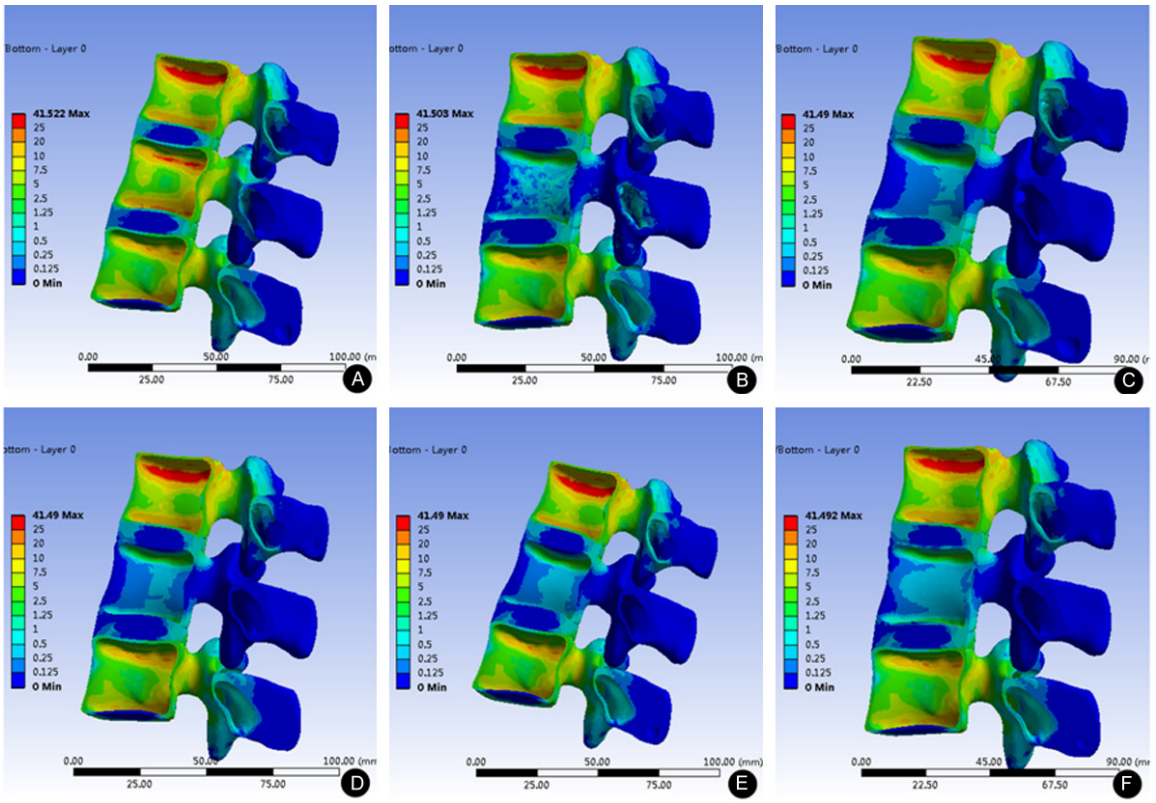

Figure 4. Von Mises stress distributions in the cortical bone of models with different cavity sizes under 260 N of axial pressure and 10 Nm of bending torque. A. No cavity, B. 1/5 cavity, C. 2/5 cavity, D. 3/5 cavity, E. 4/5 cavity, and F. 5/5 cavity.

Table 5. Von Mises equivalent stresses in different vertebral regions during flexion for different cavity locations (MPa)

Center of sphere	Von Mises equivalent stress (Quartiles)				*P* value
	Leading hemisphere		Trailing hemisphere		
	Number of nodes	Equivalent stress	Number of nodes	Equivalent stress	
1/3 before the sagittal diameter	102	1.6090 (0.5154, 2.9578)	99	0.3075 (0.1864, 0.9035)	P<0.001
Center of vertebra	98	0.6023 (0.1987, 1.2089)	103	0.5423 (0.2002, 1.0253)	P>0.5
1/3 after the sagittal diameter	90	0.3163 (0.1912, 0.8879)	101	1.6978 (0.5321, 2.9768)	P<0.001

Table 6. Von Mises equivalent stresses in different vertebral regions during bending for different cavity locations (MPa)

Center of sphere	Von Mises equivalent stress (Quartiles)				*P* value
	Upper hemisphere		Lower hemisphere		
	Number of nodes	Equivalent stress	Number of nodes	Equivalent stress	
1/3 before the vertical diameter	98	0.9544 (0.2024, 1.7317)	110	0.2875 (0.1779, 0.9210)	P<0.001
Center of vertebra	100	0.5963 (0.1758, 1.2142)	97	0.5001 (0.2101, 1.0879)	P>0.5
1/3 after the vertical diameter	99	0.3021 (0.1798, 0.8065)	101	0.9053 (0.1982, 1.8063)	P<0.001

than that in the normal vertebra (**Figure 1B-E**; where blue indicates low and red high equivalent stress). The general comparison of the Von Mises equivalent stress in the cancellous bone

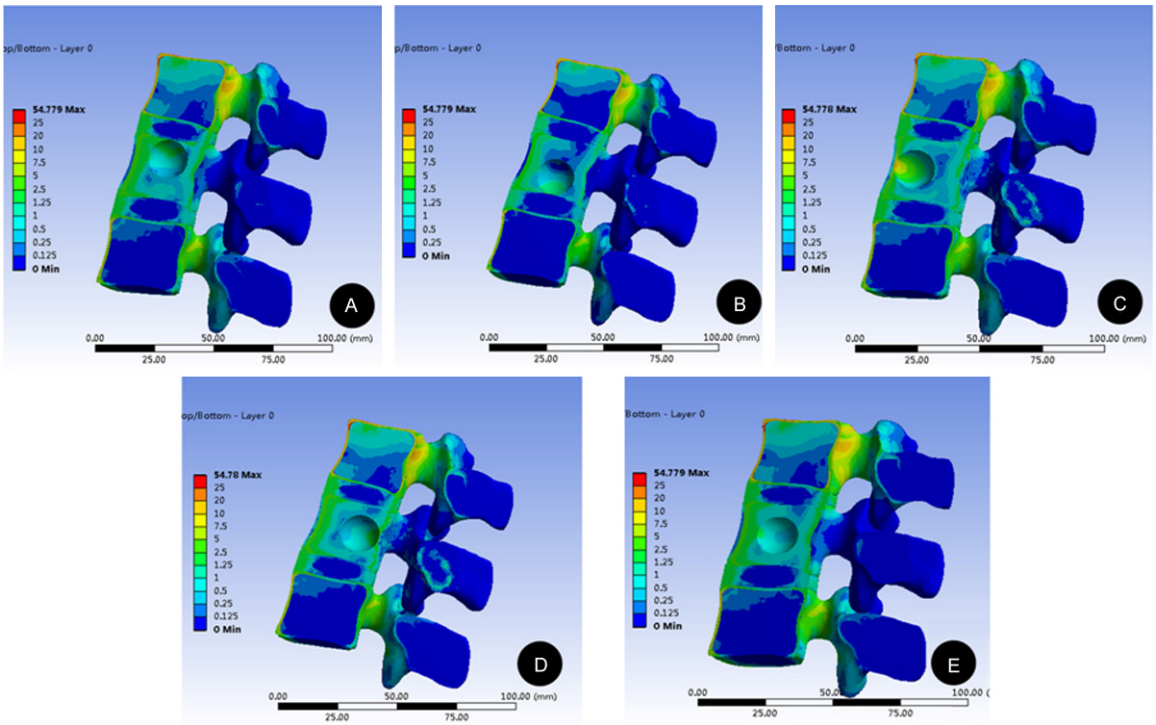

Figure 5. Von Mises stress distributions in the cancellous bone of models with different cavity locations under 260 N of axial pressure and 10 Nm of bending torque. The cavity location is 1/3 above (A) and below (B) the vertical diameter of the L2 vertebra. (C, D) The cavity location is 1/3 before (C) and after (D) the sagittal diameter of the L2 vertebra. (E) The cavity location is at the center of the vertebra.

among the six spinal models using the multiple independent samples Kruskal-Wallis H test showed a statistically significant difference ($P < 0.001$). The paired comparisons between groups using Mann-Whitney U tests indicated that the stresses in all of the cavity-like groups were significantly different than that in the normal group (all $P < 0.001$; **Table 3** and **Figure 3**). The equivalent stress in the cancellous bone gradually increased with increasing cavity volume.

The Von Mises equivalent stress in the cortical bone in the cavity-like vertebra was lower than that in the normal vertebra (**Figure 1B-E**). The general comparison of the Von Mises equivalent stress in the cortical bone among the six spinal models using the multiple independent samples Kruskal-Wallis H test showed a statistically significant difference ($P < 0.001$). The paired comparisons between groups using Mann-Whitney U tests indicated that the stresses in all of the cavity-like groups were significantly different than that in the normal group (all $P < 0.001$; **Table 4** and **Figure 4**). The equivalent stress in the cortical bone gradually increased with increasing cavity volume.

For cases with the same cavity size, the general comparison of the Von Mises equivalent stress at all nodes of the hemispheres of the the cavity among the different cavity locations using a multiple independent samples Kruskal-Wallis H test showed a statistically significant difference ($P < 0.001$). The paired comparisons between groups using Mann-Whitney U tests indicated statistically significant differences at the edges ($P < 0.001$), but not in the center ($P > 0.5$; **Tables 5**, **6** and **Figure 5**). The stress was concentrated in the cancellous bones adjacent to the endplates and vertebral edges when the cavity was close to the vertebral superior or inferior endplates, as well as when it was close to the leading or trailing edges of the vertebra.

Discussion

Effects of post-traumatic vertebral osteonecrosis on the stresses in the cortical and cancellous bones

The stress distribution in the normal vertebra shows that the Von Mises equivalent stress in the cortical bone was significantly higher than that in the cancellous bone. However, the

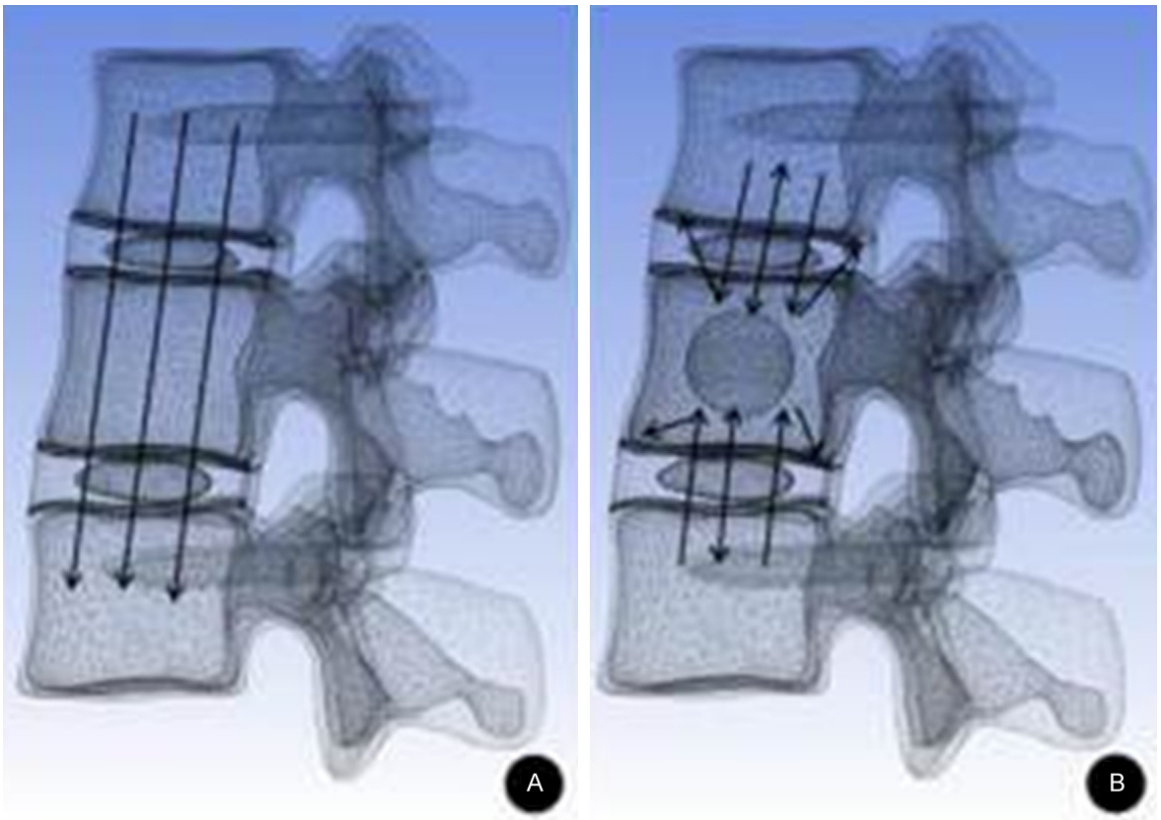

Figure 6. Illustration of the stress blocking phenomenon in the cavity-like vertebra, which appears in the cavity wall and affects the normal transmission of force in the vertebra. A. Force transmission in a normal vertebra. B. Force transmission in a cavity-like vertebra.

equivalent stress in the vertebra appears to have been significantly altered by the inclusion of a cavity in the vertebra. In that model, the equivalent stress in the cancellous bone was significantly increased, while the equivalent stress in the cortical bone was significantly reduced compared with the normal vertebra. This pattern of equivalent stress changes is known as reverse distribution of the vertebra. This reverse distribution may be explained by the cavity in the vertebra altering the normal transmission of force in cancellous bone such that the stress tends to concentrate because of the larger elastic modulus compared with the air in the cavity, generating a stress blocking effect and resulting in the increased equivalent stress in the cancellous bone (**Figure 6**). However, post-traumatic vertebral osteonecrosis likely does not alter the stress distributions on the adjacent superior and inferior vertebrae, leaving the total stress in each vertebral level unchanged. The increased stress in the cancellous bone tends to reduce the stress in the cortical bone in the cavity-like vertebra, producing the reverse distribution of the vertebral stress. With increasing cavity volume, the stress exerted per unit volume of the cancellous bone in the cavity-like vertebra is increased, but the effective volume experiencing the stress is reduced. This volume reducing trend is larger than the stress increasing trend per unit volume, leading to an overall reduced total stress on the cancellous bone. Therefore, the stress on the cortical bone in the cavity-like vertebra gradually increases with increasing cavity volume. When the cavity is positioned close to the superior or inferior endplates, the nearby vertebra tends to exhibit increased deformation, resulting in a more significant stress-blocking effect in the cancellous bone near the endplate.

Effects of the vertebral cavity on the loss of the corrective angle in the posterior approach

Although it reportedly displays a high rate of internal fixation failure, short segment pedicle instrumentation via the posterior approach is a

common treatment for thoracolumbar fractures [15, 16]. The anterior column plays a large (80%) role in maintaining stability, while the posterior column makes a smaller contribution of less than 20% [17]. In most cases of thoracolumbar fracture, the anterior column shows the most severe damage because of the mechanism of injury. Therefore, the vertebral cavity is often located in the anterior portion of the vertebra. Although the posterior pedicle instrumentation can successfully restore the vertebral height using distraction reduction, the mounting structure of the bone trabeculae in the vertebra cannot be regenerated at the same time, resulting in ineffective anterior mounting. Failure to quickly reconstruct or restore this architecture can lead to fatigue fractures of the posterior internal fixation and leaves the tissue prone to vertebral collapse after extraction of the internal fixation. Furthermore, the presence of a vertebral cavity may change the normal stress transmission in the spine, and an abnormal stress distribution will likely accelerate the degeneration of any damaged vertebrae, leading to an eventual loss in the corrective angle.

Limitations and perspective

Clinically, cavities in the cavity-like vertebrae tend to be irregularly shaped. A sphericalycavity was used in the present study, which may not accurately model the stress distributions in real vertebrae. In future studies, we plan to conduct CT follow-ups in patients with thoracolumbar fracture to identify the relationships between geometry and location of the cavity in cavity-like vertebrae and the types of vertebral fracture. In addition, we plan to develop more accurate models through statistical analysis of the major geometries and locations of the cavities within the vertebrae.

After post-traumatic osteonecrosis, cancellous bone tends to experience larger Von Mises equivalent stresses than those in normal vertebrae. Meanwhile, larger cavity volumes and locations closer to the superior or inferior endplates may result in even more abnormal stress distributions. These stress variations likely accelerate the degeneration of the vertebra and could be a risk factor for the loss of the vertebral corrective angle after extraction of the internal fixation during treatment for thoracolumbar fractures.

Disclosure of conflict of interest

None.

Address correspondence to: Dr. Pengcheng Wang, Orthopaedic Trauma Service Center, Third Hospital of Hebei Medical University, Major Laboratory of Orthopaedic Biomechanics in Hebei Province, Shijiazhuang 050051, China. Tel: +86-1773692-0525; Fax: +86-0311-88602002; E-mail: yixueshengxiaozhu@163.com

References

[1] Kümmell H. Die raretizierende Ostitis der Wirbelkörper. Deutselse Med 1895; 21: 180-181.

[2] Matzaroglou C, Georgiou CS, Panagopoulos A, Assimakopoulos K, Wilke HJ, Habermann B, Panos G and Kafchitsas K. Kümmell's Disease: Clarifying the Mechanisms and Patients' Inclusion Criteria. Open Orthop J 2014; 8: 288-297.

[3] Pappou IP, Papadopoulos EC, Swanson AN, Cammisa FP Jr and Girardi FP. Osteoporotic vertebral fractures and collapse with intravertebral vacuum sign (Kümmel's disease). Orthopedics 2008; 31: 61-66.

[4] Wang XY, Dai LY, Hua-Zi X, Chi YL, Jiang SD and Xin-Feng L. Biomechanic character and anterior reconstruction significance posterior to internal fixation of various extents of anterior median spine fractures of thoracolumbar vertebrae. Chinese Journal of Trauma 2006; 3: 214-217.

[5] Stabler A, Schneider P, Link TM, Schops P, Springer OS, Durr HR and Reiser M. Intravertebral vacuum phenomenon following fractures: CT study on frequency and etiology. J Comput Assist Tomogr 1999; 23: 976-980.

[6] Park WM, Park YS, Kim K and Kim YH. Biomechanical comparison of instrumentation techniques in treatment of thoracolumbar burst fractures: A finite element analysis. J Orthop Sci 2009; 14: 443-449.

[7] Su YS, Ren D and Wang PC. Comparison of biomechanical properties of single-segment and two-segment fusion for Denis type B spinal fracture. Orthop Surg 2013; 5:266-273.

[8] Wang H, Wang X, Chen W, Zhao F, Xiang L, Zhou Y and Cheng C. Biomechanical comparison of interspinous distraction device and facet screw fixation system on the motion of lumbar spine: a finite element analysis. Chin Med J (Engl) 2014; 127: 2078-2084.

[9] Yamamoto I, Panjabi MM, Crisco T and Oxland T. Three-dimensional movements of the whole lumbar spine and lumbosacral joint. Spine (Phila Pa 1976) 1989; 14: 1256-1260.

[10] Chen CS, Cheng CK, Liu CL and Lo WH. Stress analysis of the disc adjacent to interbody fusion in lumbar spine. Med Eng Phys 2001; 23: 483-491.
[11] Yan J, Wu Z, Wang X, Xing Z, Song H, Zhao Y, Zhang J, Wang Y and Qiu G. Finite element analysis on stress change of lumbar spine. Zhonghua Yi Xue Za Zhi 2009; 89: 1162-1165.
[12] Zeng ZL, Cheng LM, Zhu R, Wang JJ and Yu Y. [Building an effective nonlinear three-dimensional finite-element model of human thoracolumbar spine]. Zhonghua Yi Xue Za Zhi 2011; 91: 2176-2180.
[13] Yan L, Chang Z, Xu Z, Liu T, He B and Hao D. Biomechanical effects of bone cement volume on the endplates of augmented vertebral body: A three-dimensional finite element analysis. Chin Med J (Engl) 2014; 127: 79-84.
[14] Xu G, Fu X, Du C, Ma J, Li Z and Ma X. Biomechanical effects of vertebroplasty on thoracolumbar burst fracture with transpedicular fixation: A finite element model analysis. Orthop Traumatol Surg Res 2014; 100: 379-383.
[15] Alvine GF, Swain JM, Asher MA and Burton DC. Treatment of thoracolumbar burst fractures with variable screw placement or Isola instrumentation and arthrodesis: case series and literature review. J Spinal Disord Tech 2004; 17: 251-264.
[16] Alanay A, Acaroglu E, Yazici M, Oznur A and Surat A. Short-segment pedicle instrumentation of thoracolumbar burst fractures: does transpedicular intracorporeal grafting prevent early failure? Spine (Phila Pa 1976) 2001; 26: 213-217.
[17] Kopperdahl DL, Morgan EF and Keaveny TM. Quantitative computed tomography estimates of the mechanical properties of human vertebral trabecular bone. J Orthop Res 2002; 20: 801-805.